nature communications

Article

https://doi.org/10.1038/s41467-025-57699-5

PTN activity in quiescent neural stem cells mediates Shank3 overexpression-induced manic behavior

Received: 29 May 2024

Accepted: 28 February 2025

Published online: 11 March 2025

Check for updates

Hongwon Kim[1,2], Byounggook Cho[1], Hyung Kyu Kim[3], Soi Kang[1], Saemin An[1], Daeyeol Kwon[1], Hee Young Kim[3] & Jongpil Kim[1]

Mania is a complex psychiatric disease characterized by hyperactivity, elevated mood and reduced anxiety. Despite extensive studies on the mechanism of the manic episodes, the molecular targets that control manic pathogenesis remain largely unclear. Here, through single-cell RNA sequencing (scRNA-seq) analysis, we show aberrant adult neurogenesis due to increased numbers of quiescent neural stem cells (qNSC) in a manic mouse model with Shank3 overexpression. Particularly, we found that the excessive Pleiotrophin (PTN), released by dysregulated qNSCs, is a key factor contributing to the manic-like phenotypes in Shank3-overexpressing mouse models. Pharmacological and molecular inhibition of PTN in qNSCs rescued aberrant neurogenesis and effectively alleviated the manic-like social deficits observed in Shank3-overexpressing mice. Taken together, our findings present an approach for modulating PTN activity in qNSCs, proposing it as a promising therapeutic target for manic development.

Mania, a prominent symptom of bipolar disorder, is a complex psychiatric condition characterized by distinct behavioral changes including hyperactivity, elevated mood, and reduced anxiety[1,2]. Despite its prevalence and the significant impact, it has on the quality of life for affected individuals, the molecular mechanisms underlying manic behavior remain largely elusive. Various environmental and genetic factors have been linked to an increased risk of mania[3], making it particularly challenging to identify the molecular targets that control mania development.

Recently, several lines of evidence have suggested that abnormal neurodevelopment has been implicated in the onset of neuropsychiatric disorders, such as mania or bipolar disorder. For example, abnormal neural development accompanied by reduced REST levels was observed in both cerebral organoids derived from bipolar patients and in bipolar postmortem prefrontal cortex[4]. A disruption in hippocampal neurogenesis was also identified in a mouse model of bipolar disorder with manic-like behavior[5,6]. Additionally, it has been reported that altered brain volume occurs due to abnormal neurodevelopment in individuals in bipolar patients[7,8]. Moreover, alterations in plasma miRNA levels detected in bipolar individuals with manic have been shown to influence gene expression linked to neurodevelopment and neurogenesis[9].

The *SHANK3* gene encodes a synaptic scaffolding protein critical for synapse formation and function, located at the postsynaptic density of excitatory synapses. Mutations or deletions in *SHANK3* are strongly associated with various neurological disorders, including autism[10–12]. Thus, these genetic alterations can lead to symptoms such as impaired social interactions, intellectual disabilities, and developmental delays[13,14]. Beyond autism, SHANK3 has been implicated in other conditions such as bipolar disorder, highlighting the gene's broad impact on neuropsychiatric diseases. For example, in transgenic mice overexpressing SHANK3, manic-like behaviors were observed, through its role in synaptic signaling and its interaction with the mTORC1 pathway[15,16]. Moreover, recently, we have been identified the relationship between the SHANK3 and the development of autism mediated by aberrant neurogenesis[17]. In this study, we observed

[1]Department of Chemistry, Dongguk University, Pildong-ro 1-gil 30, Jung-gu, Seoul 04620, Republic of Korea. [2]Department of Chemistry and Chemical Biology, Rutgers, The State University of New Jersey, Piscataway, NJ 08854, USA. [3]Department of Physiology, Yonsei University College of Medicine, Seoul 03722, Republic of Korea. e-mail: jpkim153@dongguk.edu

SHANK3 deficiency leads to increased dormancy of quiescent neural stem cells (qNSCs), reducing neurogenesis and contributing to ASD development, suggesting that targeting qNSC activity could be a potential therapeutic strategy for autism related to *SHANK3* mutations. Given the role of SHANK3 in qNSC activity in ASD, it is plausible that SHANK3 overexpression could contribute to the development of bipolar disorder through the dysregulated neurogenesis. Therefore, exploring SHANK3's role in NSC regulation could unveil important insights into its potential involvement in the mechanisms driving bipolar disorder.

In this study, we sought to explore how adult NSCs can contribute to the onset of manic symptoms in a mouse model with Shank3 overexpression. Based on our scRNA-seq data, we initially characterized anomalies in adult neurogenesis resulting from dysregulated qNSCs in Shank3-overexpressed mice brain and their association with manic-like behaviors. In particular, we found that excess Pleiotrophin (PTN) released from qNSCs play a crucial role in manic-like symptoms observed in Shank3-overexpressing mouse models. Previously, PTN is a developmentally expressed growth factor that plays a significant role in various biological processes such as cell growth, differentiation, and survival[18]. It is involved in the regulation of neurite outgrowth, angiogenesis, and can act as a growth factor in the nervous system and other tissues[19,20]. Thus, our finding underscores the importance and role of PTN from qNSCs in adult neurogenesis, expanding its association with the pathogenesis of neuropsychiatric disorders. Interestingly, we observed that molecular inhibition of the PTN in qNSCs reinstated adult neurogenesis and alleviated manic-like social deficits observed in Shank3-overexpressed mice. This suggests a new approach to alleviate manic behaviors by regulating PTN activity from qNSCs. Thus, our findings suggest that qNSCs, the least differentiated neural stem cells during adult neurogenesis, play a key role in neurological diseases including mania. Taken together, the compelling interplay between PTN, qNSCs, and manic behavior uncovered in this study provides significant insights on the modulation of qNSC activity, proposing it as a promising therapeutic target for manic development.

Results

Abnormal adult neurogenesis in Shank3-Overexpression manic mice model

Previously, overexpression (OE) of the *SHANK3* gene has been identified as a major risk factor for Mania[16], as evidenced by manic-like conditions observed in mouse models[21]. Initially, we studied the transcriptional dynamics of adult neurogenesis in the subventricular zone (SVZ) of 8-week-old Shank3 OE mice using scRNA-seq profiling to examine whether it contributes to manic behaviors. After integrating the scRNA-seq datasets, we identified and re-clustered neural stem cell (NSC) types in control and Shank3 OE mice, classifying them into four neurogenic categories based on NSC markers[22]: quiescent neural stem cells (qNSCs), active neural stem cells (aNSCs), transient amplifying precursors (TAPs), and neuroblasts (NBs) (Fig. S1a, b, Fig. 1a–d). We analyzed neurogenic patterns to trace cell lineages in Shank3 OE adult mouse brains using pseudotime analysis with the Slingshot package[23]. Interestingly, the neurogenic lineage, showing the transcriptional dynamics from qNSCs to Neuroblasts revealed an increased number of qNSCs and a reduced number of aNSCs and Neuroblasts clusters in Shank3 OE brains (Figs. 1e, f and S1c). To investigate whether these phenotypic alterations in neurogenic density are due to changes in the mitotic activity of the qNSC and aNSCs, we performed Gene Set Enrichment Analysis (GSEA) of mitotic cell phase transition signature in control and Shank3 OE NSCs. Surprisingly, the genes associated with mitotic cell signature exhibited negative enrichment in the Shank3 OE NSCs (Fig. 1g). Consistently, in the module scoring analysis of deep quiescent NSC characteristics[24], qNSCs in Shank3 OE exhibited a higher signature score compared to the control, suggesting that aberrant neurogenesis was induced from the enhanced qNSCs state, resulting in the reduced neurogenic potentials in manic mice overexpressing Shank3 (Fig. 1h, i).

To validate the abnormal neurogenesis and enhanced activity of qNSCs in Shank3 OE manic mice, we conducted immunofluorescence assays to examine the adult neurogenic process in the SVZ and SGZ regions of 10-week-old Shank3-overexpressed mice. Consistent with previous reports, we first confirmed a significant increase in the expression of Shank3 in SVZ region of Shank3 OE mice brain (Fig. S2a). Moreover, within the SVZ region, we confirmed a significant increase in the number of Gfap + /Sox2 + /Id2+ and Gfap + /Nestin + /Sox2+ qNSCs in the brains of Shank3 OE mice (Fig. 2a–c). Also, there was a significant increase in the number of Gfap + /Sox2 + /Ki67-, Gfap + /Sox2 + /Dlx2-, and Gfap + /Nestin + /EdU- qNSCs, while the number of Gfap + /Sox2 + /Ki67+ and Gfap + /Sox2 + /Dlx2+ aNSCs decreased in Shank3 OE mice (Fig. 2d–g, and i). Furthermore, we observed a significant reduction in the number of Dcx + /EdU+ neuroblasts and Dcx + /EdU- postmitotic neuroblasts in the SVZ region of mice with Shank3 overexpression (Fig. 2h and j). Consistently, in the SGZ region of Shank3 OE mice, there was a significant increase observed in the number of qNSCs, specifically Gfap + /Nestin + /Sox2+ radial glial cells (Fig. 2k, l). But, the number of aNSCs, characterized by Gfap + /Nestin + /Sox2+ non-radial glial cells as well as Ki67 + /EdU + , and Dcx + /Psa-ncam+ cells, were significantly diminished in Shank3 OE mice compared to the control group (Fig. 2m–p). In addition, a decrease in the number of Dcx + , Ki67- postmitotic neuroblasts and Dcx + , Ki67+ mitotic neuroblasts was observed in the SGZ region of mice overexpressing Shank3 (Fig. 2q and S3a), indicating aberrant adult neurogenesis in the manic brain with Shank3 overexpression. To further examine the regenerative potential of NSCs from qNSCs, we performed a pulse-chase experiment using EdU to label NSCs during adult neurogenesis. After 7 days post-injection of EdU, we also found the reduced number of EdU + , Dcx+ neuroblasts in Shank3 OE mice (Figs. 2r, S3b). In addition, after 21 days post-temozolomide treatment, which aimed to eliminate total NSCs, the number of aNSCs in control mice recovered to ~80% of the baseline, whereas the recovery was limited to around 50% of the baseline in Shank3 OE mice (Figs. 2s, t, S4a and S5a). However, we confirmed that there was no significant change in the overall qNSC population between Shank3 OE and control mice after TMZ treatment (Fig. S4b, c). These findings suggest the impaired recovery capacity in Shank3 OE mice appears to be related to this dormancy of qNSCs rather than a loss of qNSCs during TMZ treatment.

PTN from enhanced qNSC activity in Shank3-overexpressed mice

While most qNSCs remain dormant in the NSC niche, they undergo cycles of quiescence and self-renewal depending on requirements, which are controlled by cell-cell signaling molecules[25,26]. Hence, we initially explored NSC interactions using CellChat[27] in Shank3 overexpression. We found qNSCs exhibited strong interactions not only with other cell types but also among themselves by quantifying their receptor-ligand interactions (Fig. 3a). Moreover, in these interactions, pleiotrophin (PTN) pathway was highly enriched in the NSCs of Shank3 overexpressing mice suggests an important role for PTN signaling pathway in the context of Shank3-overexpressing mania (Fig. 3b). Additionally, we confirmed the significant increase in enhanced PTN signaling across both inbound and outbound interactions in the context of Shank3 overexpression (Fig. 3c).

PTN is a secreted growth factor that its roles span from facilitating brain development and maintaining homeostasis to promoting tissue regeneration, neurogenesis upon the specific cell types and the diversity of receptors[19,20]. Thus, we next assessed the expression levels of various signaling ligand-receptor pairs to identify the interactions between qNSCs and other NSCs, under both control conditions and with Shank3 overexpression. Consistently, we found that the

https://doi.org/10.1038/s41467-025-57699-5

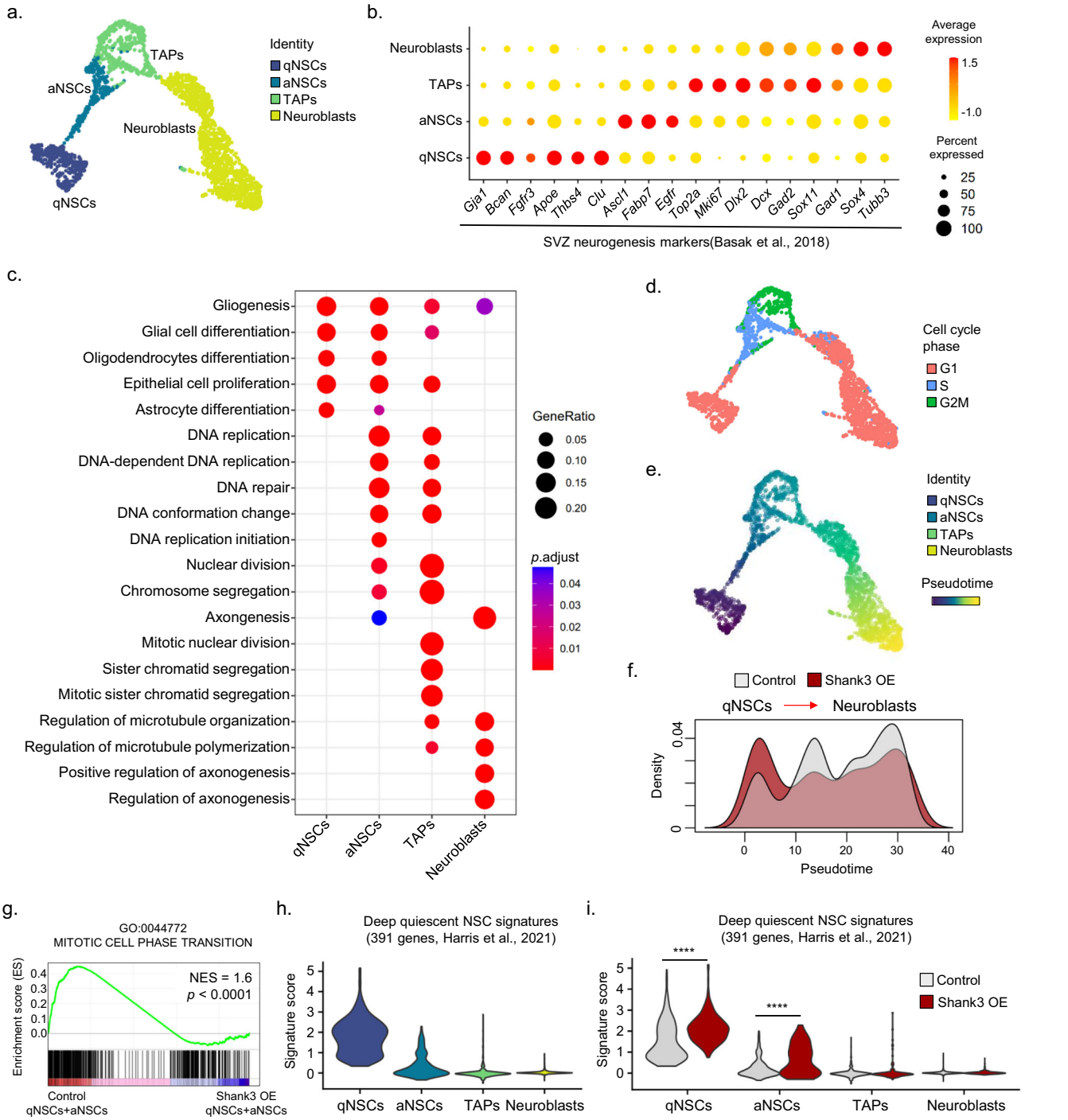

Fig. 1 | Identification of aberrant neurogenesis in Shank3 overexpressed manic-like mouse model. a UMAP visualization of 2515 cells, color-coded into four neural cell types in mouse SVZ region. **b** A dot plot validates the neural cell types using public NSC signatures[22]. **c** Dot plot of enriched pathways determined from representative NSCs. Two-tailed *t*-test. **d** UMAP plot showing cell cycle scoring analysis in neural stem cells of control and Shank3 OE mice. **e** Continuous trajectory projection using a UMAP plot generated by Slingshot, showing neurogenic lineages of NSCs. **f** Density plot representing the neurogenic trajectory across conditions. **g** GSEA plots showing that Mitotic cell phase transition signature. $p < 0.0001$; NES = 1.6, one-tailed *t*-test. **h**, **i** Violin plot presenting module scores for deep quiescent states in four neural stem cell clusters in (**h**) and comparing expression across conditions in (**i**) (Deep quiescence signature x qNSCs: $p < 2.22 \times 10^{-16}$, Deep quiescence signature x aNSCs: $p = 9.2 \times 10^{-7}$, ****$p < 0.0001$; one-tailed *t*-test). SVZ: Subventricular zone; GSEA: Gene set enrichment analysis.

interactions between NSCs involving PTN-Ptprz1 receptor, or PTN-Ncl receptors exhibited a higher probability of communication in the context of Shank3 overexpression (Figs. 3d, e and S6a–c). We further confirmed increased PTN expression within qNSCs in the Shank3-overexpressed brain, along with an elevated number of PTN-expressing qNSCs (Gfap + /Sox2 + /PTN+ and Nestin + /Sox2 + /PTN +) in the SVZ and SGZ regions of Shank3-overexpressed mice (Fig. 3f–i). PTN expression levels show no difference in Aldh1l1+ astrocytes and Iba1+ microglia between control and Shank3-overexpressing mice (Fig. S7a, b). Taken together, these findings indicate that PTN-mediated signaling in qNSCs is activated and may contribute to the abnormal neurodevelopment observed in Shank3 overexpression.

https://doi.org/10.1038/s41467-025-57699-5

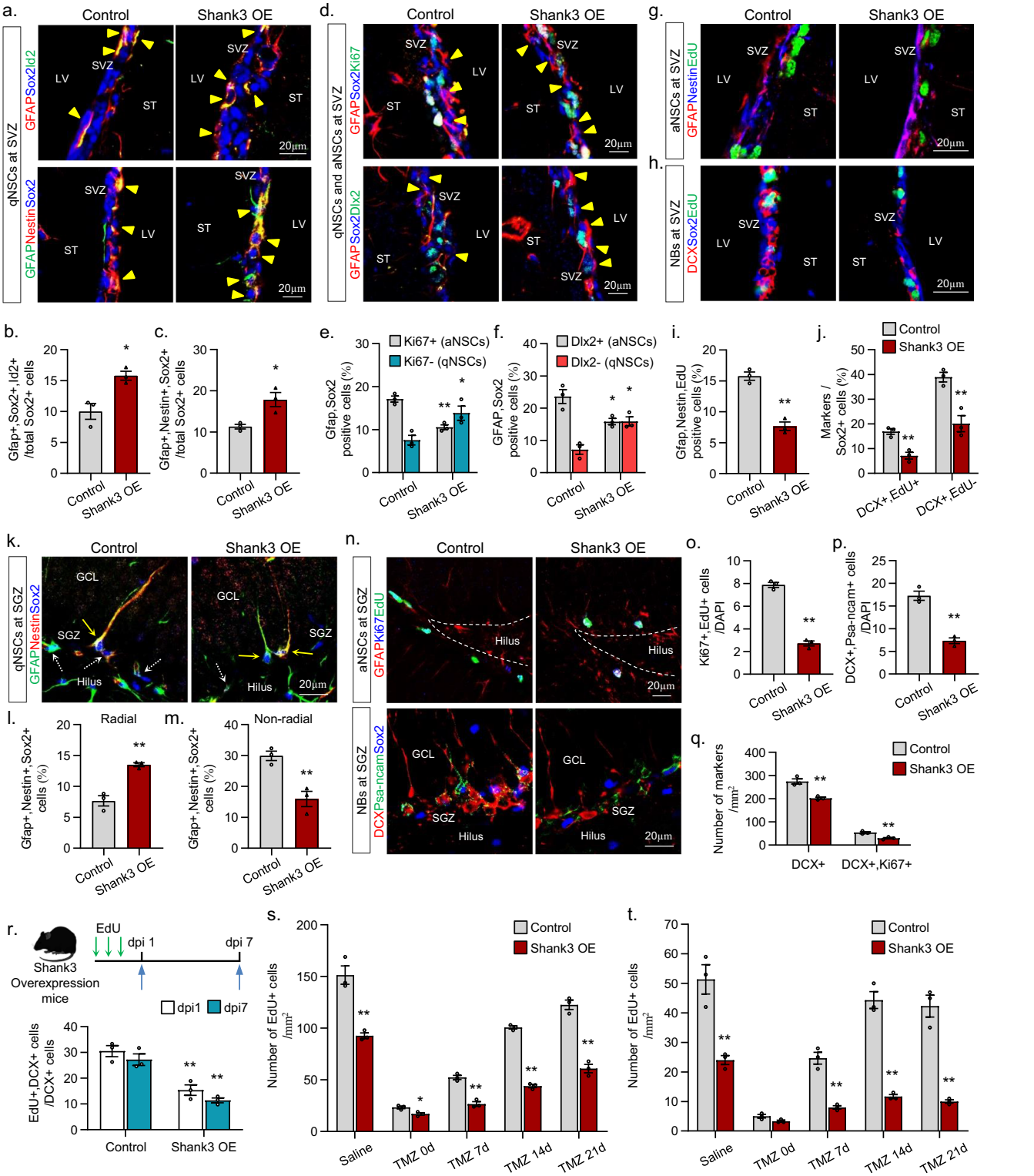

Inhibition of PTN from qNSCs restored adult neurogenesis and ameliorated Manic-like social deficits in Shank3-overexpressed mice

To investigate whether PTN functionally contributes to Shank3 OE-associated manic phenotypes and aberrant neurogenesis, we examined whether manic phenotypes and aberrant neurogenesis in Shank3 OE could be rescued by inhibiting PTN. Seven days after injecting *Ptn*-shRNA into the lateral ventricle (LV) of 8-week-old Shank3-overexpressing mice, we observed that inhibiting Ptn led to a significant reduction in the number of Gfap + /Sox2 + /Ptn+ NSCs indicating effective PTN inhibition in qNSCs (Fig. S8a). Accordingly, we observed a reduction in the number of qNSCs expressing Gfap + /Sox2 + /Dlx2- and Gfap + /Nestin + /Sox2+ in the Shank3-overexpressing mice brain following *Ptn* shRNA treatment (Fig. 4a–d, S9a, b). Consistently, in the dentate gyrus (DG) of Shank3-overexpressing mice, we found a decrease in the number of radial glia-like qNSCs expressing Gfap + /Sox2 + /NeuN- and Sox2 + /Nestin+ qNSCs and an increase in Ki67 + /Nestin+ aNSCs (Figs. 4e–h, S9c, d). Furthermore, we observed an increased number of EdU and DCX-positive cells in the SVZ and DG regions of Shank3-overexpressing

Fig. 2 | Validation of qNSCs activity in the SVZ and dentate gyrus of Shank3 overexpression mice. a Immunofluorescence for Gfap + , Sox2 + ,Id2+ (up) and Gfap + ,Nestin + ,Sox2+ (bottom) qNSCs in SVZ of control mice and Shank3 overexpressing mice. Triangular arrows indicate Gfap + ,Sox2 + , Id2+ and Gfap + , Nestin + ,Sox2+ qNSCs. **b**, **c** Quantification of qNSCs; Gfap, Sox2, and Id2-expressing cells, Gfap, Nestin, and Sox2-expressing cells. $n = 3$ per genotype. **d** Immunostaining of qNSCs in the SVZ of control mice and Shank3 overexpressing mice. Triangular arrows indicate Gfap + ,Sox2 + ,Dlx2- and Gfap + ,Sox2 + ,Dlx2- qNSCs. **e** Quantification of Gfap + ,Sox2 + ,Ki67- and Gfap + ,Sox2 + ,Ki67+ cell fractions among the total Sox2+ cells. $n = 3$ per genotype. **f** Quantification of Gfap + ,Sox2 + ,Dlx2- and Gfap + ,Sox2 + ,Dlx2+ cell fractions among the total Sox2+ cells. $n = 3$ per genotype. **g**, **h** Immunofluorescence for Gfap + ,Nestin + ,EdU+ aNSCs (**g**) and Dcx+ and EdU+ cells (**h**) in the SVZ of control mice and Shank3 overexpressing mice. **i** Quantification of Gfap + ,Nestin + ,EdU+ aNSCs. $n = 3$ per genotype. **j** Quantification of Dcx + ,EdU+ and Dcx + ,EdU- cell fractions among the total Sox2+ cells. $n = 3$ per genotype. **k** Immunofluorescence for Gfap + ,Nestin + , Sox2+ NSCs in the SGZ of control mice and Shank3 overexpressing mice. Solid arrows indicate Gfap + ,Nesin + ,Sox2+ RGs and dashed arrows indicate Gfap + , Nesin + ,Sox2+ non-RGs. **l**, **m** Quantification of RGs and non-RGs in the SGZ of control mice and Shank3 overexpressing mice. $n = 3$ per genotype. **n** Expression of Ki67 + ,EdU+ and DCX + ,Psa-ncam+ cells. **o**, **p** Quantification of Ki67 + ,EdU+ and DCX + ,Psa-ncam+ cells. $n = 3$ per genotype. **q** Number of DCX+ neuroblasts and DCX + ,Ki67+ mitotic neuroblasts. $n = 3$ per genotype. **r** Quantification of EdU + , DCX+ cells at 7 days after the final EdU administration. $n = 3$ per genotype. Graphic was created in BioRender. Kim, H. (2025) https://BioRender.com/a74w734; license for publication obtained and used in accordance with BioRender's CC-BY publishing and reader permissions. **s**, **t** Quantification of EdU positive cells in the SVZ (**s**) and SGZ (**t**) of control mice and Shank3 overexpressing mice at various time points following TMZ injection. $n = 3$ per genotype. **a**, **d**, **g**, **h**, **k**, and **n**: Scale bar = 20 μm. **b**, **c**, **e**, **f**, **l**, **j**, **l**, **m**, **o**, **p**, **q**, **r**, **s**, and **t**: Data are expressed as mean ± SEM, $^{*}p < 0.05$, $^{**}p < 0.01$; Unpaired two-tailed *t* test. Source data and *p*-values are provided as a Source Data file. RGs: Radial glia cells; TMZ: Temozolomide.

mice following *Ptn* shRNA treatment (Figs. 4i, j, S10a, b). Additionally, we confirmed that PTN inhibition resulted in a significant reduction in total branch points in retrovirus-GFP-expressing newborn neurons of Shank3-overexpressing mice, suggesting that the inhibition of PTN rescues the aberrant synaptic development observed in the condition of Shank3 overexpression (Fig. 4k). We also found that axonogenesis, nerve branching pathways are enriched in the neuroblasts of Shank3 OE mice by GSEA analysis, providing evidence that the morphological changes observed in Fig. 4k are indeed accompanied by transcriptional alterations (Fig. S10c).

Since PTN has been known to function through several putative transmembrane receptors, such as protein tyrosine phosphatase, receptor type Z1 (Ptprz1), nucleolin (Ncl), and anaplastic lymphoma kinase[28], we next investigate which receptor mediates the abnormal neurogenesis by secretion of PTN in Shank3-overexpressed mice. Interestingly, we found that knockdown of Ptprz1 and Alk, but not Ncl, led to significant increases in the numbers of Gfap + /Nesin + /Sox2+ qNSCs, but decreased in the number of Ki67 + /Nestin+ aNSCs (Fig. S11a–d). Collectively, these data suggest that knockdown of PTN effectively rescues the abnormal quiescence of qNSCs and corrects aberrations of adult neurogenesis in the Shank3 overexpressing condition.

Next, we sought to determine whether manic-like social behavior could be rescued by PTN knockdown in the Shank3 overexpressing mice. We found that the increased locomotor activity in Shank3-overexpressed mice was significantly reduced in Shank3-overexpressed mice upon *Ptn* shRNA treatment (Fig. 4i, S12a). Moreover, the duration of immobility during the tail-suspension test and forced swim test, which has been used as indicator of manic-like behavior[29], was ameliorated in Shank3-overexpressed mice upon *Ptn* shRNA treatment (Fig. 4m, n). Importantly, we found that *Ptn* shRNA treatment dramatically increased social investigation times and social preference in the three-chamber social interaction assay in Shank3-overexpressed mice compared to controls (Fig. 4o, p and S12b). These results suggest that manic-like behaviors could be controlled by inhibiting PTN expression during neurogenesis.

To elucidate the functional effects of Ptn expression in qNSCs of Shank3-overexpressing mice, a qNSC or astrocytes-specific knockdown lentivirus were prepared using a CRISPR-Cas9 plasmid driven by the *Hes1* or *Aldh1l1* promoter (Fig. S13a–c). Three weeks after injecting the qNSC-targeting Ptn knockout virus into the neurogeneic regions of Shank3-overexpressing mice, a decrease in the number of qNSCs co-expressing Gfap + /Nestin + /Sox2+ was observed, accompanied by an increase in Ki67 + /Nestin+ aNSCs (Fig. S13d–e, h). Similarly, within the SGZ region, we identified a decrease in the number of radial glia-like qNSCs expressing Gfap + /Sox2+ and an increase in Gfap + /Sox2+ non-radial glial NSCs (Fig. S13f, g). Additionally, the number of DCX-positive cells in the SVZ and SGZ regions was significantly elevated in Shank3-overexpressing mice following *Hes1* promoter-driven Ptn knockout (Fig. S13h). In contrast, Ptn knockout mediated by the astrocyte-specific *Aldh1l1* promoter did not alter the number of qNSCs, aNSCs, or neuroblasts in Shank3-overexpressing mice, indicating a specific increase in neurogenic activity linked to qNSCS-mediated Ptn knockout (Fig. S13d–h). Furthermore, Ptn knockout specifically in Hes1-expressing qNSCs markedly ameliorated manic-like social behaviors in Shank3-overexpressing mice, whereas PTN knockout in Aldh1l1-expressing astrocytes produced no significant behavioral changes (Fig. S13i). These findings suggest that Ptn secretion from qNSCs specifically contributes to aberrant neurogenesis and manic-like phenotypes observed under Shank3 overexpression conditions. However, our findings on the role of PTN in qNSCs and its potential involvement in bipolar-like behaviors present an intriguing contrast to recent studies on PTN in normal adult hippocampal neurogenesis. While Li et al.[30] demonstrated that PTN promotes adult hippocampal neurogenesis through PTPRZ1-AKT signaling in NSCs, our bipolar disorder mouse model exhibits a different relationship between PTN levels and neurogenic outcomes. This apparent discrepancy highlights the complex and context-dependent nature of PTN signaling in neurogenesis and mood regulation. The altered neurogenic environment in our bipolar model may lead to a dysregulation of the PTN-PTPRZ1-AKT pathway, resulting in abnormal neurogenesis and contributing to bipolar-like symptoms. In order to examine this hypothesis, first, we confirmed that PTN levels in qNSCs are different between our bipolar model and wild-type controls (Fig. 3f–i). Moreover, inhibition of PTN specifically in qNSCs of our bipolar model rescues abnormal neurogenesis and bipolar-like behaviors (Fig. S13). Additionally, we showed the different activation levels of AKT in our model's qNSCs indicating the downstream signaling was altered (Fig. S11e). Thus, these results suggested the differential effects of PTN in our bipolar model compared to normal adult neurogenesis, underscoring the importance of studying disease-specific contexts when investigating neurogenic mechanisms in complex neuropsychiatric disorders such as bipolar disorder.

Treatment of TAE684 rescues aberrant neurogenesis and ameliorated Manic-like behaviors in Shank3 overexpression mice

Our results indicate potential therapeutic approaches for treating Shank3-associated mania, driven by the increased activity of PTN in qNSCs and can be targeted with a specific PTN signaling inhibitor. Hence, we examined whether TAE684, a PTN-ALK receptor inhibitor[31], can rescue aberrant neurogenesis and ameliorate manic-like behaviors in Shank3-overexpressing mice. Initially, we found that the administration of TAE684 to Shank3-overexpressing mice resulted in a significant increase in aNSCs expressing Dlx2+/Sox2+ and EdU+, as well as decrease in qNSCs expressing Gfap + /Nestin + /Sox2 + (Figs. 5a–c, S14a–d). Furthermore, the number of Gfap + /Sox2+ radial glial-like

https://doi.org/10.1038/s41467-025-57699-5

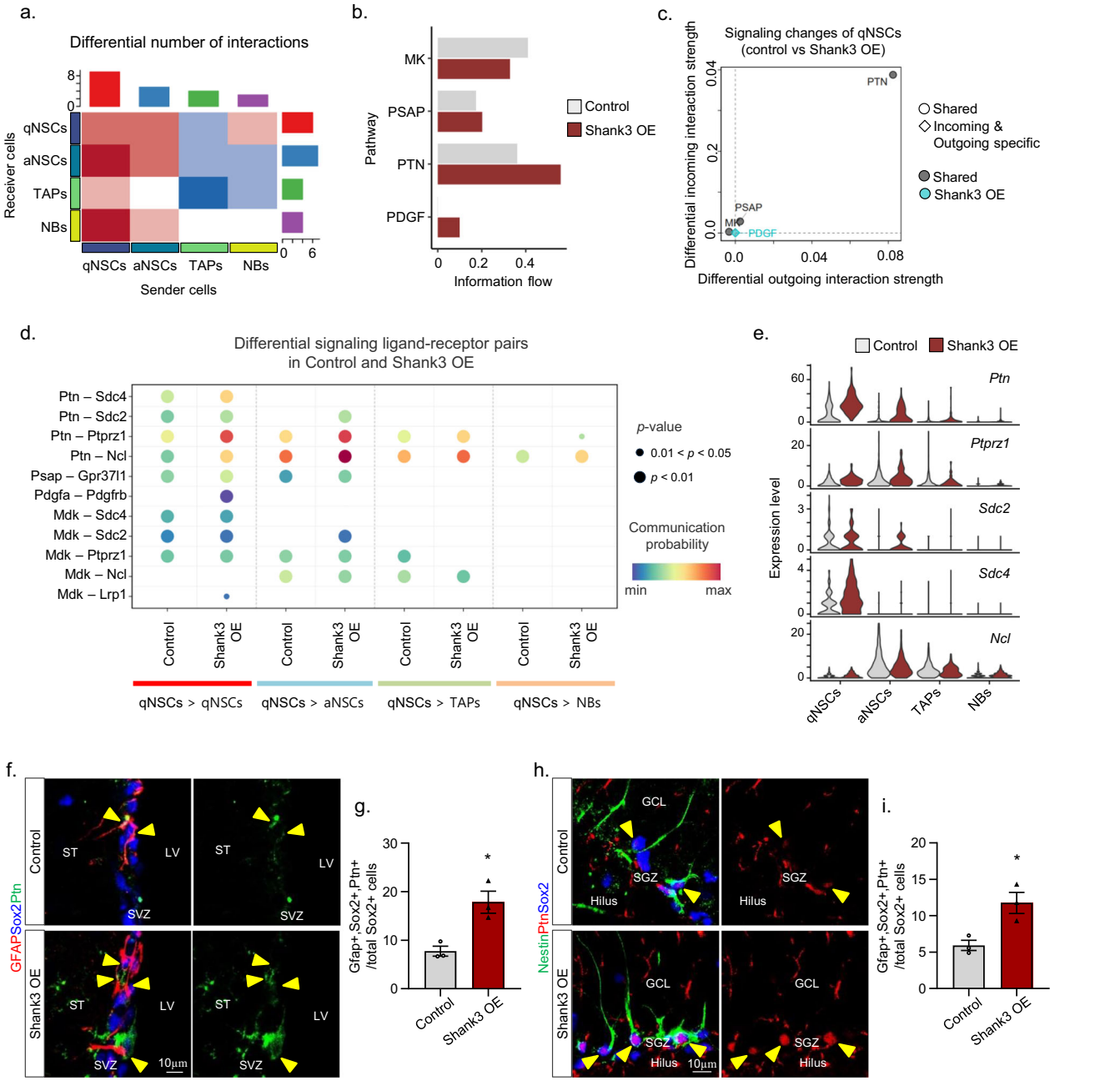

Fig. 3 | PTN signaling changes in qNSCs of Shank3 overexpression mice. **a** Heatmap showing differential number of interactions. columns; incoming interaction number, rows; outgoing interaction number. **b** Bar plot showing ranked significant signaling pathways based on differences in the overall information flow within the inferred networks between control and Shank3 OE mice. **c** Comparing the outgoing and incoming interaction strength in a 2D space. Specific signaling changes of qNSCs between control and Shank3 OE mice. **d** The ligand-receptor pairs shown in the bubble plot from qNSCs to other neural stem cell types. Two-tailed *t*-test. **e** Violin plot presenting expression of PTN-related ligand and receptor in neural stem cell types. **f** immunofluorescence for Gfap + ,Sox2 + ,PTN+ qNSCs in the SVZ of control mice and Shank3 overexpressing mice. Triangular arrows indicate Gfap + ,Sox2 + , PTN+ qNSCs. Scale bar = 10 μm. **g** Quantification of Gfap + , Sox2 + ,PTN+ cell fractions among the total Sox2+ cells. Data are expressed as mean ± SEM, $n = 3$ per genotype, $^*p < 0.05$, two-tailed *t* test. **h** Immunofluorescence for Nestin + ,Sox2 + ,PTN+ RGs in the SGZ of control mice and Shank3 overexpressing mice. Triangular arrows indicate Nestin + ,Sox2 + , PTN+ qNSCs. Scale bar = 10 μm. **i** Quantification of Gfap + ,Sox2 + ,PTN + RG fractions among the total Sox2+ cells. Data are expressed as mean ± SEM, $n = 3$ per genotype, $^*p < 0.05$; Unpaired two-tailed *t*-test. Source data and *p*-values are provided as a Source Data file.

qNSCs was decreased, while the number of Gfap + /Sox2+ and EdU+ active NSCs was increased in the SGZ of Shank3-overexpressed mice following TAE684 treatment (Figs. 5d–f, S14c, d). Consistently, following TAE684 treatment, the number of Dcx + /Ki67- post-mitotic neuroblasts and Dcx + /Ki67+ mitotic neuroblasts increased in Shank3 overexpressing mouse brain (Fig. S15a, b). Collectively, these findings suggest that TAE684 treatment inhibits the PTN-ALK-associated pathway in the Shank3-overexpressing brain, consequently reinstating normal adult neurogenesis. Moreover, 2 weeks after TAE684 administration, a decreased number of VGLUT1-positive puncta was partially rescued in Shank3-overexpressed mice, while the increased GAD65/67-positive puncta was diminished compare to control mice (Fig. 5g, h). Consistent with these findings, we observed a reduction in the imbalanced GAD65+ neurons/ VGLUT1+ neurons ratio in Shank3-overexpressed mice (Fig. 5i). Moreover, in Shank3-overexpressing mice treated with TAE684, we observed significant

https://doi.org/10.1038/s41467-025-57699-5

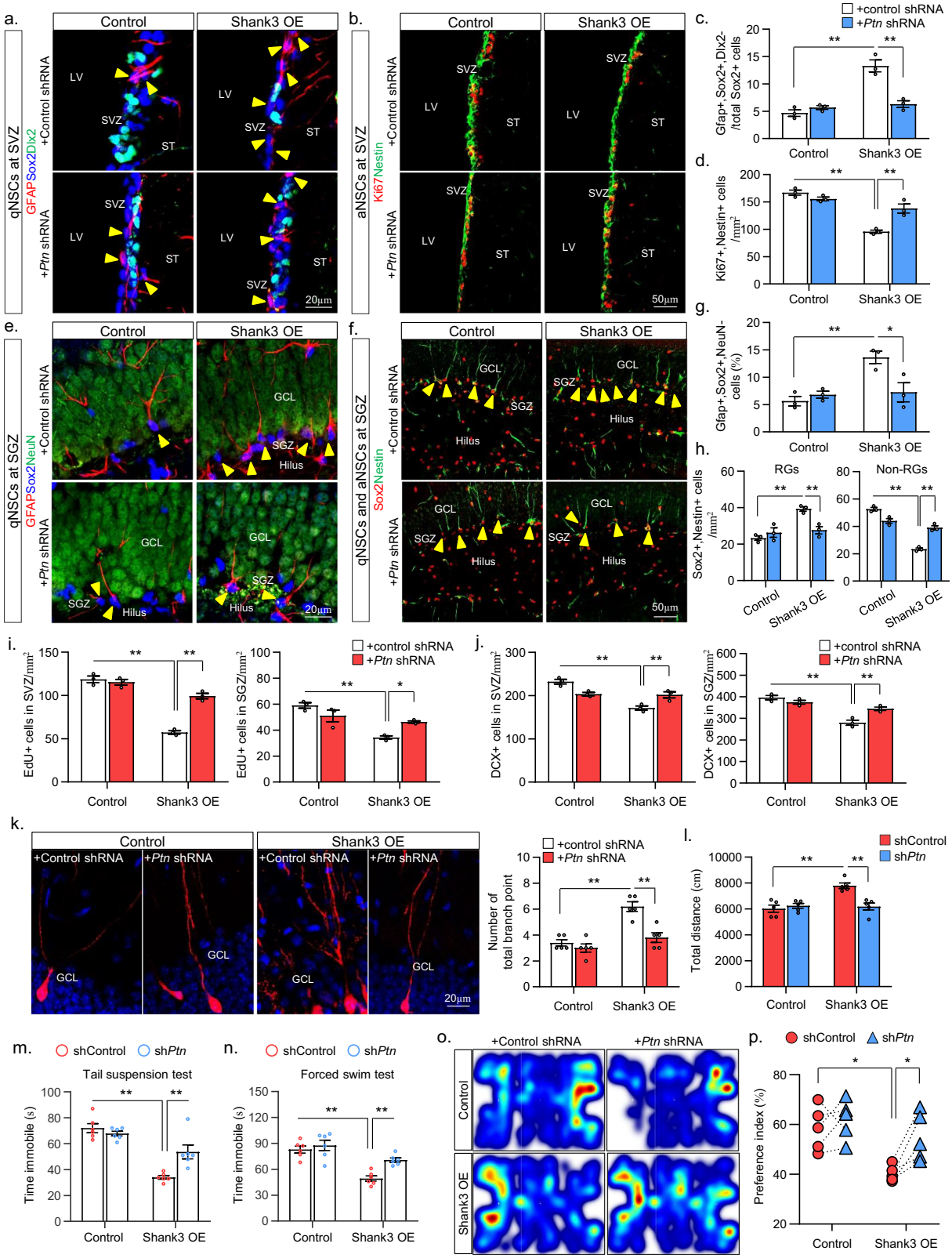

restoration of the inhibitory synaptic protein GABRBR1 and the excitatory synaptic protein VGLUT2. (Figs. 5j, S16a). Additionally, elevated levels of synaptic scaffolding proteins such as SAPAP3 and PSD95 were also restored following treatment with TAE684 (Fig. 5k). Consistently, we confirmed that Shank3-overexpressing mice treated with TAE684 displayed a reduced amplitude of sEPSCs, when compared to untreated Shank3-overexpressing mice (Fig. S16b, c). Importantly, the abnormal E/I ratio was also restored in Shank3-overexpressing mice after TAE684 treatment (Fig. S16d), demonstrating that the pharmacological effects of TAE684 can rectify the imbalance between excitation and inhibition of synaptic activity in the brains of Shank3 overexpressing mice. Thus, our findings suggest a complex role for PTN in the development of bipolar-like symptoms in our Shank3 overexpressing mouse model. While we initially focused on the impact

Fig. 4 | Knockdown of PTN rescues manic-like pathology in Shank3 overexpression mice. a Immunofluorescence for qNSCs in SVZ of control and Shank3 overexpressing mice treated with *PTN* shRNA. Triangular arrows indicate Gfap+, Sox2+, Dlx2- qNSCs. Scale bar = 20 μm. **b** Immunofluorescence for Nestin+, Ki67+ aNSCs in SVZ of control and Shank3 overexpressing mice treated with *PTN* shRNA. **c**, **d** Quantification of Gfap + ,Sox2 + ,Dlx2- qNSCs and Nestin + ,Ki67+ aNSCs. $n = 3$ per genotype. **e** Immunostaining of RGs in the SGZ of control and Shank3 overexpressing mice treated with *PTN* shRNA. Triangular arrows indicate Gfap + , Sox2 + , NeuN- qNSCs. Scale bar=20 μm. **f** Immunostaining of Nestin + , Sox2+ cells. Triangular arrows indicate Nestin + ,Sox2+ RGs. Scale bar = 50 μm. **g** Quantification of Gfap + ,Sox2 + ,NeuN- qNSCs. $n = 3$ per genotype. **h** Quantification of Nestin + ,Sox2+ RGs and Nestin + ,Sox2+ non-RGs fractions among the total Sox2+ cells. $n = 3$ per genotype. **i** Quantification of EdU+ NSCs among SVZ and SGZ treated with *Kmt2a*-shRNA after a 3-h EdU pulse. Control and Shank3 overexpressing mice treated with *Kmt2a*-shRNA were injected intraperitoneally with a daily dose of EdU (100 mg/kg/day). $n = 3$ per genotype. **j** Quantification of Dcx+ cells in the SVZ and SGZ of control and Shank3 overexpressing mice treated with *PTN* shRNA. $n = 3$ per genotype. **k** Representative images of RFP-retrovirus expressing newborn neurons in control and Shank3 overexpressing mice treated with *PTN* shRNA. Number of branch points in RFP-expressing newborn neurons from control and Shank3-overexpressing mice treated with *PTN* shRNA, measured 7 days post-treatment with RFP-retrovirus. Scale bar=20 μm. $n = 5$ per genotype. **l**–**n** Behavioral analysis of open field test (**l**), tail suspension test (**m**), and force swim test (**n**) in control and Shank3-overexpressing mice, measured 21 days post-treatment with *PTN* shRNA. $n = 5$ per genotype. **o** Representative heat maps showing the time spent in 3 chambers to assess the social behavior. **p** Social preference index percentages in control and Shank3-overexpressing mice treated with *PTN* shRNA after 21 days. $n = 5$ per genotype. **c**, **d**, **g**, **h**, **i**, **j**, **k**, **l**, **m**, **n**, and **p**: Data are expressed as mean ± SEM, $^{*}p < 0.05$, $^{**}p < 0.01$; two-way ANOVA with Tukey's post hoc test. Source data and *p*-values are provided as a Source Data file.

of abnormal neurogenesis, the rapid improvement in manic-like behaviors following TAE684 injection (within 2–3 weeks) (Fig. S18), indicates that PTN may have more immediate effects on neural function. We propose that PTN expression in qNSCs could modulate excitatory and inhibitory (E/I) synaptic function through paracrine signaling. This hypothesis is supported by recent studies demonstrating that NSCs influence their local microenvironment through secreted factors or growth factors, may directly affect synaptic proteins, alter neurotransmitter balance, activate glial cells, or rapidly change neuronal excitability in the surrounding mature neurons[32,33]. Thus, while our data still support a role for PTN in neurogenesis, we now recognize that its effects on synaptic function may be more immediate and directly relevant to the behavioral changes observed in our model. Future studies are need to dissect these dual roles of PTN in both neurogenesis and rapid synaptic modulation, providing a more comprehensive understanding of its involvement in bipolar-like symptoms.

Furthermore, we used TAE684 to determine the therapeutic impact of inhibiting the PTN receptor, leading to the reversal of manic-like behaviors in the Shank3-overexpressed mice. Three weeks after TAE684 administration, in Shank3-overexpressed mice, TAE684 reduced locomotor activity in the open field, reduced latency to immobility in the tail-suspension test and forced swim test (Fig. 5l, m, S17a). However, other antipsychotic drug, clozapine, had no significant effects (Fig. 5l, m, S17a). Interestingly, we found that in the Shank3 overexpression, mice treatment of TAE684, but not clozapine, led to the normalization of time spent in the social stimuli (Fig. 5n–p, S17b).

While SVZ neurogenesis is primarily associated with olfactory functions and the SGZ neurogenesis is linked to learning, memory, and emotion, recent evidences suggest that SVZ neurogenesis also play a role in social behavior and mood regulation[34–36]. Thus, altered SVZ neurogenesis in Shank3 overexpressing mice could indirectly influence emotional circuits by modulating olfactory processing, which has connections to limbic areas involved in mood regulation. So, in order to investigate the impact of TAE684 on neurogenesis and manic-like behavior in the SVZ and SGZ of Shank3-overexpressing mice, we performed stereotaxic injections of TAE684 into the SVZ, SGZ, or both SVZ/SGZ regions separately. Three weeks after administering TAE684, we observed a marked increase in the population of aNSCs co-expressing Ki67 + /Nestin+ (Fig. S18a, b) when TAE684 was injected into the SGZ alone or both SVZ and SGZ regions. Consistently, TAE684 injection into these neurogenic regions of Shank3-overexpressing mice significantly alleviated manic-like behaviors, with the most substantial improvements observed in the SGZ and combined SVZ/SGZ treatments (Fig. S18c–e). These findings suggest that TAE684 selectively mitigates manic-like phenotypes in Shank3-overexpressing mice, particularly when targeting the SGZ or both neurogenic regions. This highlights its potential role in modulating aberrant neurogenesis and manic-associated behaviors driven by Shank3 overexpression, with the SGZ emerging as a key target for intervention. Taken together, controlling PTN activity secreted from qNSCs with TAE684 is a promising therapeutic strategy for rescuing manic-like behaviors in Shank3-overexpressed conditions.

Discussion

Manic, a significant psychiatric disorder, is marked by symptoms such as hyperactivity, elevated mood, and decreased anxiety[37]. Traditional treatments offer partial relief but fail to cure the condition, underscoring the critical need for new therapeutic strategies. Many studies have investigated the role of abnormal synaptic functions and plasticity in neuropsychiatric disorders, including manic[38–40]. However, the impact of adult neurogenesis and adult NSCs on the development of manic remains unclear, despite suggestions of their association with neuropsychiatric diseases.

In this study, we demonstrate that the aberrant qNSC activity and its secreted factor PTN could be a crucial target for controlling phenotypes associated with manic episodes induced by Shank3 overexpression. Through single-cell RNA sequencing analysis, we identified significant alterations in adult neurogenesis in a manic mouse model with Shank3 overexpression, specifically attributing these changes to enhanced dormancy activity in qNSCs or impaired transition to aNSCs. Thus, our findings extend the previous observations by revealing a potential link between dysregulated qNSCs and bipolar disease, highlighting the role of qNSCs's role in neuropsychiatric pathophysiology. The inherent dormancy of qNSCs enables them to await specific activation signals before becoming active. This regulatory mechanism plays a crucial role in maintaining brain plasticity and facilitating repair processes, but can be frequently disrupted in neuropsychiatric disorders. However, the observed enhancement in qNSC numbers presents an intriguing interpretation of qNSC dynamics. Rather than a simple problem with exiting dormancy, the accumulation of qNSCs may be attributed to a transition issue. Specifically, there could be a bottleneck in the progression from the quiescent to the activated state, leading to an apparent increase in qNSC numbers. This hypothesis consists with recent studies highlighting the complexity of NSC state transitions[41]. Furthermore, we can speculate that qNSCs may need to exit the cell cycle to transition effectively, a process potentially blocked by PTN. This interpretation is also supported by emerging evidence on the role of cell cycle regulators in NSC fate decisions[42]. Thus, in this regard, it's important to note that our observations differ from those in knockout studies. Future studies should focus on elucidating the precise mechanisms governing the transition between quiescent and activated NSC states. Additionally, investigating the interplay between PTN, cell cycle regulators, and NSC state transitions may reveal new therapeutic targets for neurological disorders associated with aberrant NSC function.

https://doi.org/10.1038/s41467-025-57699-5

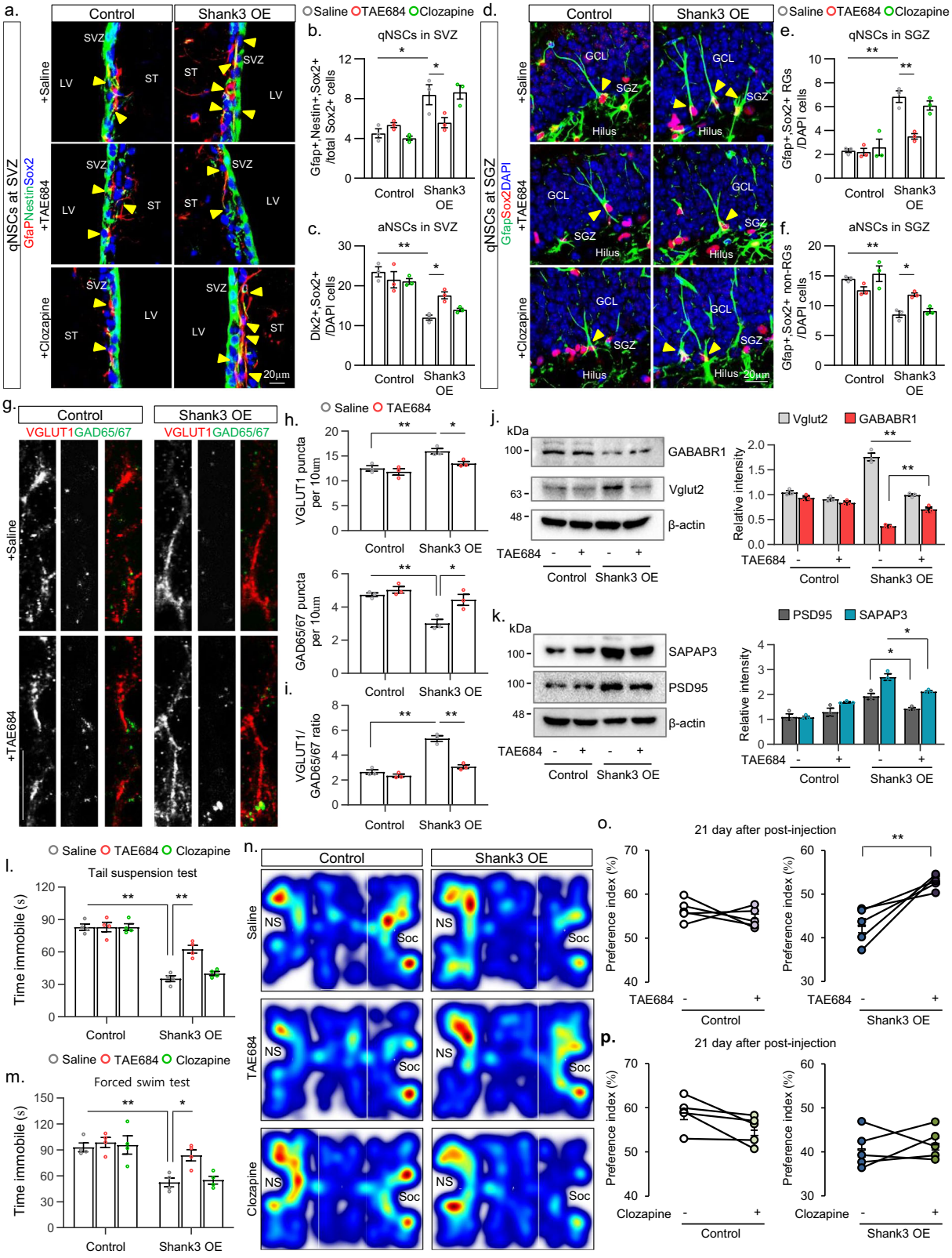

Additionally, we showed that alterations in the microenvironment of qNSCs, including changes in growth factors, neurotransmitters, and inflammatory cytokines, can adversely affect neurogenesis or neurons in the adult brain. Such alternations can lead to a decrease in the production of new neurons impacting cognitive functions and emotional regulation. Consistent with this ideas, previous studies have showed a connection between the microenvironment, including growth factors and neurotrophic factors, and the development of neuropsychiatric conditions[43,44]. Particularly, we found excessive PTN release from dysregulated qNSCs contributes to the aberrant neurogenesis and manic-like social deficits observed in Shank3-overexpressing mice. Pleiotrophin (PTN) plays various roles in different organs throughout the body and is involved in processes such as cell growth, differentiation, and survival[18]. In the nervous

Fig. 5 | Treatment of TAE684 rescues manic-like pathology in Shank3 overexpression mice. a Immunofluorescence for qNSCs in the SVZ of control and Shank3 overexpressing mice sacrificed 14 days after saline, TAE684 (5 mg/kg, once daily for 5 days), and clozapine (5 mg/kg, once daily for 5 days) treatment. Triangular arrows indicate Gfap+, Nestin+, Sox2+ qNSCs. **b**, **c** Quantification of Gfap+, Nesin+, Sox2+ qNSCs and Dlx2 + ,Sox2+ aNSCs in the SVZ of control and Shank3 overexpressing mice injected with each drug. $n = 3$ per genotype. **d** Immunofluorescence for Gfap+, Sox2+ cells in the SGZ of control and Shank3 overexpressing mice sacrificed 14 days after saline, TAE684, and clozapine treatment. Triangular arrows indicate Gfap+, Sox2+ RGs. **e**, **f** quantification of Gfap+, Sox2+ RGs and Gfap+, Sox2+ Non-RGs. $n = 3$ per genotype. **g** Immunofluorescence for VGLUT1 and GAD65/67 cells in the SGZ of control and Shank3 overexpressing mice injected with saline and TAE684. **h**, **i** Quantification of VGLUT1 and GAD65/67-positive puncta (**h**), and the ratio of excitatory to inhibitory synapses (**i**) in the SGZ of control and Shank3 overexpressing mice injected with saline and TAE684. $n = 3$ per genotype. **j** Western blot analysis of GABABR1 and Vglut2 in the dentate gyrus from control or Shank3 overexpressing mice injected with saline or TAE684. $n = 3$ per genotype. **k** Relative intensity of synaptic scaffolding proteins of the dentate gyrus. $n = 3$ per genotype. **l**, **m** Behavioral analysis of tail suspension test (**l**), and force swim test (**m**) in control and Shank3-overexpressing mice, measured 21 days post-treatment with saline, TAE684, and clozapine. $n = 4$ per genotype. **n** Representative heat maps showing the time spent in 3 chambers to assess the social behavior in Control and Shank3-overexpressing mice injected with saline, TAE684, and clozapine. **o**, **p** Social preference index percentages in control and Shank3-overexpressing mice injected with each drugs after 21 days. $n = 5$ per genotype. **a**, **d** and **g**: Scale bar = 20 μm. **b**, **c**, **e**, **f**, **h**, **l**, **j**, **k**, **l**, **m**, **o**, and **p**: Data are expressed as mean ± SEM, $^{*}p < 0.05$, $^{**}p < 0.01$; two-way ANOVA with Tukey's post hoc test. Source data and *p*-values are provided as a Source Data file.

system, PTN promotes the development and maintenance of neurons, contributing to synaptic plasticity and nerve regeneration[45]. Additionally, PTN has been implicated in angiogenesis which is crucial for tissue repair and wound healing[46]. Moreover, PTN has been found to modulate immune responses and may have implications in inflammatory conditions[47]. Consequently, we have identified an additional role of PTN functions in the neurogenesis contributing to the development of neuropsychiatric disorders, mania. However, the relationship between Shank3 overexpression and enhanced protein translation (PTN) is complex and not fully understood, but we can speculate on potential mechanisms based on Shank3's known functions as a synaptic scaffolding protein. Firstly, Shank3 might directly or indirectly interact with PTN within the cell, and its overexpression could potentially recruit or activate more of PTN. Also, cytoskeletal reorganization resulting from Shank3 overexpression might also affect the localization or efficiency of PTN expression. Moreover, Shank3 has been linked to the mTOR pathway and calcium homeostasis, and its overexpression might lead to changes in these cell signaling that indirectly affect PTN expression. Additionally, the cell might respond to Shank3 overexpression by upregulating various cellular processes, including PTN as a compensatory mechanism. Thus, it's important to note that further studies would be necessary to confirm the exact mechanisms by which Shank3 overexpression enhances PTN expression, given the complex nature of cellular signaling and the multiple roles of Shank3. We further identified that PTN interacts with a specific receptor ALK, which mediated mania phenotypes in Shank3-overexpressing mouse model. These finding underscores the importance of PTN-ALK signaling in the pathogenesis of manic behaviors and positions PTN-ALK signaling as a potential therapeutic target for neuropsychiatric disorders. Consistently, our study observed that pharmacological and molecular inhibition of PTN-ALK signaling in qNSCs effectively rescued aberrant neurogenesis and alleviated manic-like social deficits in Shank3-overexpressing mice. Further studies are necessary to elucidate the precise downstream signaling pathways and molecular interactions involved in PTN-mediated effects on other NSCs and post-mitotic neurons in the mania condition.

Moreover, while our bipolar mouse model demonstrates a potential link between abnormal neurogenesis and bipolar disease, we recognize that the extent and relevance of adult neurogenesis in the human brain, particularly in bipolar disorder, remain uncertain. Recent studies indicate that human neurogenesis may be limited primarily to early childhood, unlike the ongoing neurogenesis observed in adult rodents[48,49]. This discrepancy presents a significant challenge in directly extrapolating our findings to human bipolar disorder. However, recently, it has been reported that in the adult human brain, small populations of astrocytes may undergo dedifferentiation or cell fate conversion to a state resembling adult neural stem cells[50]. Thus, we can propose that this process could be triggered by factors associated with bipolar disorder, leading these astrocytes to secrete PTN, as observed in our mouse model. The secretion of PTN might then influence the surrounding neural environment, potentially inducing mood fluctuations characteristic of bipolar disorder without relying on extensive adult neurogenesis. This hypothesis highlights the plasticity of astrocytes and suggests a potential mechanism for how bipolar disorder could manifest in adults, warranting further investigation into qNSC behavior and PTN levels in human patients.

In conclusion, our study advances our understanding of the molecular and cellular mechanisms contributing to manic behaviors and provides a therapeutic target for the treatment of mania and related mood disorders. By targeting PTN activity in qNSCs, it may be possible to modulate aberrant neurogenesis and alleviate manic symptoms, paving the way for the development of targeted and effective treatments for bipolar disorder and other mood disorders characterized by manic episodes.

Methods

Mice and pharmacological treatment

All animal experiments were approved by the Institutional Animal Care and Use Committee at Dongguk University and performed in accordance with institutional guidelines (IACUC-2021-042-2). All mice were maintained in a controlled condition of 12 h light (8 a.m.–8 p.m.)/12 h dark (8 p.m.–8 a.m.) cycle. And all mice were kept in temperature at 22–23 °C, humidity 50-60%, and air management systems which control air flow. Mice lines were checked daily. Shank3 transgenic mice overexpress a wild-type mouse *Shank3* (*SH3/ankyrin domain gene 3*) gene and EGFP directed by *Shank3* promoter/enhancer regions on the BAC transgene. These mice (#024033) were obtained from The Jackson Laboratory. Behavior assays were conducted using 8 weeks-old control mice ($n = 5$ male mice per group) and Shank3 overexpression mice ($n = 5$ male mice per group). They were randomly assigned to experimental groups and had been backcrossed with a C57Bl/6 background for at least five generations. Mice were treated with Temozolomide (TMZ) with 50 mg/kg through intraperitoneal injection for consecutive 5 days. TMZ was dissolved in PBS + 1% BSA, which was used to treat control animals. TAE684 working solutions (5 mg/kg) were prepared by dissolving them in dimethyl sulfoxide and diluting them with 0.9% saline before intraperitoneal injection, administered once daily for 5 days at appropriate concentrations.

Behavioral test

Social behavior test. Social interaction behavioral tests were conducted in a rectangular arena with dimensions of 60 cm length, 40 cm width, and 25 cm height, housing a three-chambered box with retractable doorways for access. Two capsules were positioned in the center of each side chamber, and 8-week-old control ($n = 5$ male mice per group) and Shank3 overexpression mice ($n = 5$ male mice per group) were given a 10 min habituation period to explore the chambers. Following habituation, a nonsocial stimulus (a black block) was placed in one chamber, while a social stimulus (an age- and

sex-matched mouse of the same strain) was placed in the opposite chamber. The test mouse was then introduced into the center chamber and allowed to explore all three chambers for 10 min. Video recording captured the mouse's behavior, and specialized behavioral tracking software (EthoVision) was used to calculate the time spent exploring each chamber.

Open field test. The activity levels of mice were assessed using the open field technique, which employed a square arena measuring 40 × 40 × 40 cm and equipped with a recording setup. 8 week-old control ($n = 5$ male mice per group) and Shank3 overexpression mice ($n = 5$ male mice per group) were placed gently in the center of the arena, and recording commenced promptly. They were allowed to move around freely for 10 min. Analysis of their movement and exploration behaviors was conducted using the Smart (Ver.3.0) software program.

Tail suspension test. The experimental setup involved using a white acrylic chamber with one open side for video recording. 8 week-old control ($n = 5$ male mice per group) and Shank3 overexpression mice ($n = 5$ male mice per group) were suspended by their tails in the illuminated center of the chamber and monitored for 6 min. Their immobility episodes were recorded and analyzed using ANY-MAZE software by Stoelting Co., Ltd. Immobility was defined as any period where the mice stopped moving for at least 1 s. The duration of immobility for each mouse was recorded in seconds and then expressed as a percentage of the total time or as a percentage per minute.

Porsolt forced swim test. The setup featured four Plexiglas cylinders positioned at the center of a square chamber enclosed by white acrylic walls, with one side open for video recording. Illumination at the chamber center was set at 250 lx. 8 week-old control ($n = 5$ male mice per group) and Shank3 overexpression mice ($n = 5$ male mice per group), placed in the cylinders filled with water at 23°C, were observed for 6 min via video recording. Analysis focused on determining immobility episodes and their duration, with immobility defined as no movement for at least 1 s. Data were collected and analyzed using ANY-MAZE software by Stoelting Co., Ltd.

Viral manipulations

PTN shRNA (Target sequence: AGT CTG ACT GTG GAG AAT G, Cat. No 38124094), *Ptprz1* shRNA (Target sequence: TCA GAT AGC CTT AAT GAT AAT GAG ACG TC, Cat. No. 38190094), *Ncl* shRNA (Target sequence: GAA CGG TAA GAA TGC CAA GAA, Cat. No. 31563094), and *Alk* shRNA (Target sequence: TCA CTG GCC CTG GAT TGT GAG CCT CTG CT, Cat. No. 11771094) were procured from Applied Biological Materials Inc. Lentivirus production was conducted in HEK293FT cells cultured in Dulbecco's modified Eagle's medium supplemented with 10% fetal bovine serum and 1% penicillin/streptomycin. HEK293FT cell line was purchased from Invitrogen (Cat. no. R70007). Authentication of the cell line was performed using STR profiling, and it was confirmed to be free of mycoplasma contamination. Following previous protocols[51,52], cells were transfected with the lentiviral constructs (*Ptn* shRNA, *Ptprz1* shRNA, *Ncl* shRNA, *Alk* shRNA) along with psPAX2 and pMD2.G vectors using calcium phosphate co-precipitation method. Post-transfection, the culture medium was replaced, and the viruses were collected 48–72 h later. In vivo administration of the viral suspension (1.5 μl per side) was accomplished via bilateral stereotaxic injection into the lateral ventricle (0.5 mm anterior to bregma; ±1.5 mm lateral, 2.6 mm depth below the tissue surface) or the dentate gyrus (−2.1 mm anterior to bregma; ±1.9 mm lateral, 2.2 mm depth below the tissue surface) using a Hamilton syringe.

Immunohistochemistry

Mouse brain tissues were sectioned to 40 μm thickness using a microtome. Subsequently, brain sections were fixed in 4% paraformaldehyde in phosphate-buffered saline (PBS) and washed with PBS. Immunostaining was performed following standard protocols[53,54], utilizing primary antibodies against specific markers including Gfap (1:500, Abcam, ab53554), Sox2 (1:500, Millipore, AB5603), Nestin (1:200, Invitrogen, MA1-110, PA5-47378), Id2 (1:200, Santa Cruz, sc-398104), Dlx2 (1:200, Santa Cruz, sc-393879), Psa-ncam (1:500, Invitrogen, 14-9118-82), Dcx (1:200, Cell Signaling, 4604), NeuN (1:500, Millipore, MAB377), Ki67 (1:500, Invitrogen, 14-5698-82), Vglut1 (1:500, Invitrogen, 48-2400), GAD65/67 (1:200, Santa Cruz, sc-365180), Aldh1l1 (1:500, Abcam, ab177463), Iba1 (1:500, Abcam, ab178847), Akt (1:500, Cell Signaling, 9272S), S100 beta (1:500, GeneTex, GTX129573), PSD95 (1:200, Invitrogen, 51-6900), Vglut2 (1:500, Abcam, ab79157), and PTN (1:200, Santa Cruz, sc-74443). Fluorescent secondary antibodies (Invitrogen) were used accordingly. The sections were then mounted using Fluoromount-G mounting medium, and representative images were acquired using a confocal laser-scanning microscope (ZEISS, LSM800). We quantified the average number of immunostained cells across all samples for each experimental group. To ensure unbiased and representative sampling, quantification was performed on 10 independent sections per animal, selected at regular intervals to cover target neurogenic regions. We randomly selected 10 non-overlapping fields of view for immunostaining analysis of each section, quantified all immunopositive cells within these tissue regions, and subsequently calculated the mean cell count per field. This sampling approach was applied to 5-6 animals per group, which were randomly chosen to 3-4 animals for analysis.

Western blot analysis

Mouse brain tissues were homogenized and lysed using RIPA buffer supplemented with 1% NP-40, 0.5% DOC, 0.1% SDS, and 150 mmol/L NaCl in 50 mmol/L Tris (pH 8.0), with the addition of a 1x proteinase inhibitor mixture (GenDepot)[55,56]. Following the addition of 5x SDS loading buffer, the samples were boiled for 5 min and then centrifuged at 12000 g for 10 min. The resulting supernatants were subjected to electrophoresis on 12% sodium dodecyl sulfate-polyacrylamide gels and subsequently transferred onto 0.2 μm nitrocellulose membranes. The membrane was then probed with the following antibodies: PSD95 (1:1000, Invitrogen, 51-6900), SAPAP3 (1:1000, Cell Signaling, ABN325), GABABR1 (1:1000, Santa Cruz, 398901), Vglut2 (1:1000, Abcam, ab79157), Shank3 (1:1000, Invitrogen, MA5-27601), and β-actin (1:1000, Abfrontier, LF-PA0207).

Single cell isolation

Brain samples from control and Shank3 overexpression mice were prepared in the same single-cell isolation batch to minimize potential batch effects. The SVZ region tissues from control and Shank3 overexpression 8 week-old mice were then dissected. The microdissected subventricular zone region was cut into ~1 mm^3 pieces using sterile razor blades, following the protocols specified in the Adult Brain Dissociation Kit for the gentleMACS™ Dissociator. The resulting cell suspension was mixed with an equal volume of 0.5% BSA in DPBS (Dulbecco's Phosphate-Buffered Saline) and then filtered through a 40 μm strainer. The filtered cells were counted using the Countess 3 Automated Cell Counter and diluted to a concentration of 1000 cells/μl before being captured individually through the 10X Genomics Single-Cell 3' system. The construction of 10X libraries followed the standard protocol without any modifications. Individual single-cell cDNA libraries were combined and subsequently sequenced, with each sample generating 5 million reads, using a HiSeq 4000 sequencer.

Bioinformatic analysis

Alignment and Quality Control of scRNA-seq data: We utilized the 10X Genomics CellRanger v6.1.2 software for the analysis of all datasets. The Fastq files underwent mapping and alignment to the mouse genome (mm10) using the STAR software with default settings. Subsequently, we filtered out cells with mitochondrial gene content >10%.

Additionally, cells with unique feature counts below 500 or above 4000 were also removed from the analysis.

Dimensionality Reduction and Clustering of scRNA-seq: To integrate the datasets from both control and Shank3 overexpressed mice and identify transcriptional alterations, we employed an integrated analysis utilizing the IntegrateData function of the Seurat package (v4.3.0)[57]. We applied the non-linear dimensional reduction algorithm RunUMAP and performed cell clustering using variable genes. Additionally, we utilized the AddModuleScore function within the Seurat package module to score the deep quiescent state signature.

Molecular dynamics and pseudotime analysis: Slingshot was utilized to perform trajectory analysis. Initially, we conducted dimensional reduction using Multidimensional Scaling (MDS) on a subset of the data. Following this, Principal Component Analysis (PCA) was performed on either individual or integrated datasets. Seurat objects were then transformed into SingleCellExperiment objects. Slingshot trajectory analysis was executed utilizing the Seurat clustering information in conjunction with the dimensionality reduction obtained from MDS.

Cell–cell communication analysis: We utilized the CellChat package[27] to conduct cellular interaction analysis on neural stem cell clusters. Our objective was to compare the extrinsic signal between control and Shank3 overexpression conditions. We ran the CellChat pipeline with default settings to investigate the characteristics of cell-cell communication under both conditions. Given the relatively low number of clusters in certain groups, we employed the projectData function to project the inference results from gene expression to protein-protein interaction networks, aiming for increased reliability. Subsequently, we merged the results from the control and Shank3 overexpression datasets to facilitate comparative analyses.

Whole-cell patch-clamp recordings

All data acquisition and analyses were carried out blinded to genotype. Acute fresh hippocampal slices were prepared from 8-week-old Shank3-overexpressing mice and Shank3-overexpressing mice treated with TAE684 as previously described[16]. Horizontal brain slices (300-μm thick) containing medial hippocampus were cut with a Leica VT1200 vibratome in a chamber filled with chilled (2–5 °C) cutting solution containing (in mM) 110 choline-chloride, 25 $NaHCO_3$, 25 d-glucose, 11.6 sodium ascorbate, 7 $MgSO_4$, 3.1 sodium pyruvate, 2.5 KCl, 1.25 NaH_2PO_4 and 0.5 $CaCl_2$. The slices were then incubated in regular artificial cerebrospinal fluid (ACSF, in mM) containing 117 NaCl, 3.6 KCl, 1.2 NaH_2PO_4, 25 $NaHCO_3$, 11 glucose, 2.5 $CaCl_2$, and 1.2 $MgSO_4$, equilibrated with 95% oxygen and 5% CO2, adjusted to pH 7.3, 310 mosmol at the room temperature. Whole-cell recording was made using patchclamp amplifiers (Multiclamp 700B) under infrared–differential interference contrast microscopy (Zeiss). Data acquisition and analysis were performed using digitizers (DigiData 1550B 16-bit A/D converter) and analysis software pClamp 10.4 (Molecular Devices; Sunnyvale, CA). Signals were filtered at 1 kHz and sampled at 5 kHz. Spontaneous EPSCs (sEPSCs) and IPSCs (sIPSCs) were recorded from CA1 hippocampal pyramidal neurons in voltage-clamp mode at −70 mV and 30 mV, respectively. sEPSCs were recorded in the presence of the $GABA_A$ receptor blocker SR95531 (10 μM). Spontaneous IPSCs were recorded in the presence of AMPA and NMDA receptor antagonists, CNQX (10 μm) and DL-AP5 (50 μm), to block glutamatergic responses. Borosilicate glass pipettes (World Precision Instruments, Sarasota, FL; Sutter Instruments, Novato, CA) with a resistance of ~8 MΩ were filled with a solution containing (in mM) 120 K-gluconate, 10 KCl, 2 Mg-ATP, 0.5 Na-GTP, 0.5 EGTA, 20 HEPES, and 10 Phosphocreatine, adjusted to pH 7.3, 290-296 mOsm. All analysis was performed using pClamp software and Mini Analysis Software for event detection, frequency, and amplitude assessments.

Statistical analysis

All data are presented as the mean ± SEM, derived from three independent experiments. The sample size *n* refers to the number of independent experiments or individual mice per experiment. Each dataset comprises results from three independent sets, each containing at least three biological replicates. Statistical analyses were conducted using GraphPad Prism software. *P*-values were determined using Student's *t*-test for two-group comparisons, and one-way or two-way ANOVA with Tukey's post hoc test for multiple comparisons, followed by the Tukey-Kramer post-hoc test for pairwise comparisons. We assessed normality using the Shapiro-Wilk test. For datasets with *p*-values above 0.05, the assumption of normality was satisfied, thereby justifying the use of *t*-tests for group comparisons in the main figures (Fig. 2b, c, e, f, i, j, l, m, o, p, q, r and Fig. 3g, i). Detailed statistical parameters are provided in the corresponding figure legends and the source data.

Reporting summary

Further information on research design is available in the Nature Portfolio Reporting Summary linked to this article.

Data availability

The mouse single-cell RNA-seq datasets generated in this study have been deposited in the SRA accession numbers (SRR29354070, SRR19153375, SRR29354069). Source data are provided with this paper.

Code availability

Code used for single cell RNA-seq data is available on a GitHub repository at https://github.com/Jobang9286/PTN_qNSC_scRNAseq. The original release for this publication can be found at https://doi.org/10.5281/zenodo.14915356.

References

1. Cassidy, F., Murry, E., Forest, K. & Carroll, B. J. Signs and symptoms of mania in pure and mixed episodes. *J. Affect. Disord.* **50**, 187–201 (1998).
2. Mansell, W. & Pedley, R. The ascent into mania: a review of psychological processes associated with the development of manic symptoms. *Clin. Psychol. Rev.* **28**, 494–520 (2008).
3. Escamilla, M. A. & Zavala, J. M. Genetics of bipolar disorder. *Dialogues Clin. Neurosci.* **10**, 141–152 (2008).
4. Meyer, K. et al. Impaired neural stress resistance and loss of REST in bipolar disorder. *Mol. Psychiatry* https://doi.org/10.1038/s41380-023-02313-7 (2023).
5. Abrial, E. et al. Protein kinase C inhibition rescues manic-like behaviors and hippocampal cell proliferation deficits in the sleep deprivation model of mania. *Int. J. Neuropsychopharmacol.* **18**, pyu031 (2014).
6. Yu, Z. et al. Transmembrane protein 108 involves in adult neurogenesis in the hippocampal dentate gyrus. *Cell Biosci.* **9**, 9 (2019).
7. Hewitt, T. et al. Bipolar disorder-iPSC derived neural progenitor cells exhibit dysregulation of store-operated Ca2+ entry and accelerated differentiation. *Mol. Psychiatry* **28**, 5237–5250 (2023).
8. Hibar, D. P. et al. Cortical abnormalities in bipolar disorder: an MRI analysis of 6503 individuals from the ENIGMA bipolar disorder working group. *Mol. Psychiatry* **23**, 932–942 (2018).
9. Tabano, S. et al. A miRNome analysis of drug-free manic psychotic bipolar patients versus healthy controls. *Eur. Arch. psychiatry Clin. Neurosci.* **270**, 893–900 (2020).
10. Durand, C. M. et al. SHANK3 mutations identified in autism lead to modification of dendritic spine morphology via an actin-dependent mechanism. *Mol. Psychiatry* **17**, 71–84 (2012).
11. Zhou, Y. et al. Mice with shank3 mutations associated with ASD and schizophrenia display both shared and distinct defects. *Neuron* **89**, 147–162 (2016).
12. Qin, L. et al. Social deficits in Shank3-deficient mouse models of autism are rescued by histone deacetylase (HDAC) inhibition. *Nat. Neurosci.* **21**, 564–575 (2018).

13. Cochoy, D. M. et al. Phenotypic and functional analysis of SHANK3 stop mutations identified in individuals with ASD and/or ID. *Mol. Autism* **6**, 23 (2015).
14. Lee, D. K. et al. Reduced sociability and social agency encoding in adult Shank3-mutant mice are restored through gene re-expression in real time. *Nat. Neurosci.* **24**, 1243–1255 (2021).
15. Lee, Y. et al. Striatal transcriptome and interactome analysis of shank3-overexpressing Mice reveals the connectivity between shank3 and mTORC1 signaling. *Front. Mol. Neurosci.* **10**, 201 (2017).
16. Han, K. et al. SHANK3 overexpression causes manic-like behaviour with unique pharmacogenetic properties. *Nature* **503**, 72–77 (2013).
17. Kim, H. et al. Dormant state of quiescent neural stem cells links Shank3 mutation to autism development. *Mol. Psychiatry* **27**, 2751–2765 (2022).
18. González-Castillo, C., Ortuño-Sahagún, D., Guzmán-Brambila, C., Pallàs, M. & Rojas-Mayorquín, A. E. Pleiotrophin as a central nervous system neuromodulator, evidences from the hippocampus. *Front. Cell. Neurosci.* **8**, 443 (2015).
19. Qin, E. Y. et al. Neural precursor-Derived Pleiotrophin Mediates Subventricular Zone Invasion by Glioma. *Cell* **170**, 845–859.e819 (2017).
20. Tang, C. et al. Neural Stem Cells Behave as a Functional Niche for the Maturation of Newborn Neurons through the Secretion of PTN. *Neuron* **101**, 32–44.e36 (2019).
21. Scotti, M. A. et al. Behavioral and pharmacological assessment of a potential new mouse model for mania. *Physiol. Behav.* **103**, 376–383 (2011).
22. Basak, O. et al. Troy+ brain stem cells cycle through quiescence and regulate their number by sensing niche occupancy. *Proc. Natl Acad. Sci. USA* **115**, E610–E619 (2018).
23. Street, K. et al. Slingshot: cell lineage and pseudotime inference for single-cell transcriptomics. *BMC Genomics* **19**, 477 (2018).
24. Harris, L. et al. Coordinated changes in cellular behavior ensure the lifelong maintenance of the hippocampal stem cell population. *Cell Stem Cell* **28**, 863–876.e866 (2021).
25. Decimo, I., Fumagalli, G., Berton, V., Krampera, M. & Bifari, F. Meninges: from protective membrane to stem cell niche. *Am. J. Stem Cell* **1**, 92–105 (2012).
26. Rodriguez Lavado, J. et al. Trehalose- and glucose-derived glycoamphiphiles: small-molecule and nanoparticle toll-like receptor 4 (TLR4) modulators. *J. Med. Chem.* **57**, 9105–9123 (2014).
27. Jin, S. et al. Inference and analysis of cell-cell communication using CellChat. *Nat. Commun.* **12**, 1088 (2021).
28. Wang, X. Pleiotrophin: Activity and mechanism. *Adv. Clin. Chem.* **98**, 51–89 (2020).
29. Yu, X. et al. Dysfunction of ventral tegmental area GABA neurons causes mania-like behavior. *Mol. Psychiatry* **26**, 5213–5228 (2021).
30. Li, H. et al. Pleiotrophin ameliorates age-induced adult hippocampal neurogenesis decline and cognitive dysfunction. *Cell Rep.* **42**, 113022 (2023).
31. Galkin, A. V. et al. Identification of NVP-TAE684, a potent, selective, and efficacious inhibitor of NPM-ALK. *Proc. Natl Acad. Sci. USA* **104**, 270–275 (2007).
32. Kirby, E. D., Kuwahara, A. A., Messer, R. L. & Wyss-Coray, T. Adult hippocampal neural stem and progenitor cells regulate the neurogenic niche by secreting VEGF. *Proc. Natl Acad. Sci. USA* **112**, 4128–4133 (2015).
33. Dumitru, I., Neitz, A., Alfonso, J. & Monyer, H. Diazepam binding inhibitor promotes stem cell expansion controlling environment-dependent neurogenesis. *Neuron* **94**, 125–137.e125 (2017).
34. Pan, Y. W., Kuo, C. T., Storm, D. R. & Xia, Z. Inducible and targeted deletion of the ERK5 MAP kinase in adult neurogenic regions impairs adult neurogenesis in the olfactory bulb and several forms of olfactory behavior. *PLoS ONE* **7**, e49622 (2012).
35. Sakamoto, M. et al. Continuous neurogenesis in the adult forebrain is required for innate olfactory responses. *Proc. Natl Acad. Sci. USA* **108**, 8479–8484 (2011).
36. Feierstein, C. E. et al. Disruption of adult neurogenesis in the olfactory bulb affects social interaction but not maternal behavior. *Front. Behav. Neurosci.* **4**, 176 (2010).
37. Martino, D. J., Valerio, M. P. & Parker, G. The structure of mania: an overview of factorial analysis studies. *Eur. Psychiatry. J. Assoc. Eur. Psychiatrists* **63**, e10 (2020).
38. Lee, Y., Zhang, Y., Kim, S. & Han, K. Excitatory and inhibitory synaptic dysfunction in mania: an emerging hypothesis from animal model studies. *Exp. Mol. Med.* **50**, 1–11 (2018).
39. Maksimovic, M., Vekovischeva, O. Y., Aitta-aho, T. & Korpi, E. R. Chronic treatment with mood-stabilizers attenuates abnormal hyperlocomotion of GluA1-subunit deficient mice. *PLoS ONE* **9**, e100188 (2014).
40. Murray, G. K. et al. Substantia nigra/ventral tegmental reward prediction error disruption in psychosis. *Mol. Psychiatry* **13**, 267–276 (2008). 239.
41. Ruetz, T. J. et al. CRISPR-Cas9 screens reveal regulators of ageing in neural stem cells. *Nature* **634**, 1150–1159 (2024).
42. Cai, C. et al. c-Myc regulates neural stem cell quiescence and activation by coordinating the cell cycle and mitochondrial remodeling. *Signal Transduct. Target. Ther.* **6**, 306 (2021).
43. Autry, A. E. & Monteggia, L. M. Brain-derived neurotrophic factor and neuropsychiatric disorders. *Pharmacol. Rev.* **64**, 238–258 (2012).
44. de Miranda, A. S., de Barros, J. & Teixeira, A. L. Is neurotrophin-3 (NT-3): a potential therapeutic target for depression and anxiety? *Expert Opin. Ther. Targets* **24**, 1225–1238 (2020).
45. Blondet, B., Carpentier, G., Lafdil, F. & Courty, J. Pleiotrophin cellular localization in nerve regeneration after peripheral nerve injury. *J. Histochem. Cytochem. Off. J. Histochem. Soc.* **53**, 971–977 (2005).
46. Christman, K. L. et al. Pleiotrophin induces formation of functional neovasculature in vivo. *Biochem. Biophys. Res. Commun.* **332**, 1146–1152 (2005).
47. Fernández-Calle, R. et al. Pleiotrophin regulates microglia-mediated neuroinflammation. *J. Neuroinflam.* **14**, 46 (2017).
48. Sanai, N. et al. Corridors of migrating neurons in the human brain and their decline during infancy. *Nature* **478**, 382–386 (2011).
49. Sorrells, S. F. et al. Positive controls in adults and children support that very few, if any, new neurons are born in the adult human hippocampus. *J. Neurosci. Off. J. Soc. Neurosci.* **41**, 2554–2565 (2021).
50. Kremer, L. P. M. et al. DNA methylation controls stemness of astrocytes in health and ischaemia. *Nature* **634**, 415–423 (2024).
51. Kim, H., Lee, Y. J., Kwon, Y. & Kim, J. Efficient generation of brain organoids using magnetized gold nanoparticles. *Sci. Rep.* **13**, 21240 (2023).
52. Cho, B. et al. Epigenetic dynamics in reprogramming to dopaminergic neurons for Parkinson's disease. *Adv. Sci.* **11**, e2403105 (2024).
53. Park, H. et al. Single-cell RNA-sequencing identifies disease-associated oligodendrocytes in male APP NL-G-F and 5XFAD mice. *Nat. Commun.* **14**, 802 (2023).
54. Kim, H., Kim, S., Cho, B., Shin, J. & Kim, J. APOE ε4-dependent effects on the early amyloid pathology in induced neurons of patients with Alzheimer's disease. *Transl. Neurodegener.* **11**, 45 (2022).
55. Kim, H. et al. Administration of bifidobacterium bifidum BGN4 and bifidobacterium longum BORI improves cognitive and memory function in the mouse model of Alzheimer's disease. *Front. Aging Neurosci.* **13**, 709091 (2021).
56. Park, H. & Kim, J. Activation of melatonin receptor 1 by CRISPR-Cas9 activator ameliorates cognitive deficits in an Alzheimer's disease mouse model. *J. Pineal Res.* **72**, e12787 (2022).
57. Hao, Y. et al. Integrated analysis of multimodal single-cell data. *Cell* **184**, 3573–3587.e3529 (2021).

Acknowledgements
This work was supported by Korean Fund for Regenerative Medicine funded by Ministry of Science and ICT, and Ministry of Health and Welfare (2021M3E5E5096464; H.K., B.C., J.K.) and Basic Science Research Program through the National Research Foundation of Korea (NRF) funded by the Ministry of Education (NRF-2022R1A6A1A03053343; H.K., B.C., S.A., D.K., J.K.). This work was also supported by the ABC-based Regenerative BioTherapeutics (ABC project) grant funded by the Korea government (the Ministry of Science and ICT, the Ministry of Health & Welfare (RS-2024-00433755; H.K., B.C., J.K.)).

Author contributions
H.K. and B.C. conducted the majority of the experiments and contributed equally to this work. H.K., B.C., and S.K. performed, analyzed, and conducted the animal experiments. H.K., B.C., D.K., and S.A. performed and interpreted the bioinformatics analyses. H.K.K. and H.Y.K. conducted the whole-cell patch-clamp recordings. H.K. and J.K. developed the key concept and designed the overall study. All authors contributed to the writing of this manuscript and approved the final version.

Competing interests
The authors declare no competing interests.

Additional information
Supplementary information The online version contains supplementary material available at https://doi.org/10.1038/s41467-025-57699-5.

Correspondence and requests for materials should be addressed to Jongpil Kim.

Peer review information *Nature Communications* thanks the anonymous reviewers for their contribution to the peer review of this work. A peer review file is available.